









Periodic cellular core sandwich panel (CCSP) for bridge deck applications

Tanvir Faisal ^{a,*} , Li Hui ^b , Mohammad J. Khattak ^b , Vijaya Gopu ^{b,c} , Walid Alaywan ^c ,
Guillermo Escoto ^b 

^a Department of Mechanical Engineering, University of Louisiana at Lafayette, LA 70503, United States

^b Department of Civil Engineering, University of Louisiana at Lafayette, LA 70503, United States

^c Louisiana Transportation Research Center (LTRC), Baton Rouge, LA 70808, United States

ARTICLE INFO

Keywords:

Cellular core sandwich panel (CCSP)
Sandwich panel system (SPS)
Bridge deck
Finite element analysis (FEA)

ABSTRACT

Sandwich structures have demonstrated exceptional structural performance in different fields including automotive, aerospace, and naval industries. Cellular Core Sandwich Panel (CCSP) is a type of sandwich structure that has been widely used in weight critical structures, but not generally utilized in civil infrastructures including bridges. In this study, CCSP bridge decks were designed in accordance with the American Association of State Highway and Transportation Officials (AASHTO) Load and Resistance Factor Design (LRFD) bridge design code. This study aims to investigate the structural performance of periodic CCSP, cellular core with repeated unit cell, for bridge decks. The use of CCSP significantly reduces the dead load, and they are designed to withstand standard highway bridge loads as per AASHTO LRFD Strength I Limit State. Four cellular core topologies—double rectangle, rhombus, square, and double trapezoid were used in CCSP design, and the panels were analyzed computationally via Finite Element Analysis (FEA) for different boundary and loading conditions. The FE model with square cellular core was experimentally validated. The designed CCSPs were comprehensively assessed to investigate the influence of cellular core topologies on the static, dynamic, and buckling behavior. The unit cells designed with diagonal/inclined struts/cell walls exhibited a better stress dissipation capacity and higher structural strength than the unit cells with only vertical cell walls/struts. Finally, a high strength-to-weight ratio panel capable of effectively resisting the specified working conditions was identified. The proposed CCSP design provides an alternate and efficient engineering solution for new bridge deck construction as well as bridge deck replacement.

1. Introduction

The sandwich panel system (SPS) comprising outer plates made of high stiffness materials that enclose a low density core [1] can be a promising alternative for bridge decks, helping to meet the growing demand for renovating deteriorated bridges and [2] constructing new bridges worldwide. Fatigue failure is a common occurrence in orthotropic bridge decks resulting in a reduced lifespan and higher maintenance costs [3]. In contrast, sandwich panel decks have high fatigue endurance, provide a much higher bending stiffness than monolithic structures of similar mass, and involve lower maintenance costs [4]. In general, the SPS exhibits higher strength-to-weight ratio, stiffness-to-weight ratio, better fatigue strength, high tensile strength, high thermal and acoustic insulation, and better energy absorption and dissipation properties [5]. Hence, we hypothesize that the SPS bridge can enhance structural capacity and construction efficiency, provide

structural upgrades in bridge rehabilitation projects, and reduce total project costs and schedules.

Sandwich panels are designed to fulfill various needs, including ensuring safety, carrying loads, and absorbing energy. They provide significant benefits in sectors such as marine vessel construction, automotive engineering, and aviation, where balancing lightness and strength is crucial [6,7]. The SPS structures often exhibit extraordinary structural properties [8–10]. The mechanical effectiveness of sandwich structures in specific loading situations is heavily influenced by the core structure and its design. Ultralight and strong sandwich panel comprising cellular cores are utilized across nearly every engineering field [11,12]. The cellular core sandwich panel (CCSP) configuration for structural applications was primarily inspired by honeycomb and other cellular structures found in nature [13,14]. Furthermore, modular design and prefabrication enable efficient construction, reducing manufacturing time and costs [15], thereby increasing their potential

* Correspondence to: Mechanical Engineering, University of Louisiana at Lafayette, 241 E Lewis St., LA 70503, United States.

E-mail address: tanvir.faisal@louisiana.edu (T. Faisal).

for application in engineering structures.

One of the most critical factors in bridge design is the deadload. CCSP can reduce the dead load by more than 70 % compared to traditional concrete decks [16]. By reducing the structural weight of an existing bridge, its live load capacity can be significantly increased, ensuring a structural upgrade to meet the live load capacity demands without replacing the entire structure. The core configuration greatly affects the performance of sandwich panels and is closely intertwined with the behavior of the core design. Therefore, core topology in a CCSP plays a critical role in maintaining structural effectiveness and integrity, minimizing the weight. Topological variations in cellular core significantly influence the structural properties even at the same relative density [17, 18]. The aim of this research is to design CCSP for bridge decking that can withstand standard traffic loads effectively under typical conditions, significantly reduce the deck weight and increase the structural capacity of bridge infrastructure.

In-plane periodic cellular core sandwich panels possess high porosity with a void ratio of 80 % or more [19]. Although moisture could depreciate the structural efficiency of the struts, in-plane cellular core panels are resistant to moisture retention, which is a significant advantage in humid environments [20]. Conversely, the moisture retention in out-of-plane honeycomb and foam core sandwich panels may cause premature deterioration [21]. Furthermore, the in-plane cellular cores provide an excellent stiffness-to-weight ratio, resulting in ultralight weight panels, making them ideal for orthotropic applications where weight is the determinant factor. Hence, the objective of this study was to design CCSP bridge decks and evaluate their structural performance.

In this work, we investigated the static, dynamic, and buckling behavior of the CCSPs considering their cellular core topology. CCSPs with different core topologies (Fig. 1) were assessed for their yielding, shear, deflection, buckling, and fatigue to establish a functional relationship between core topology and the structural capacity of the sandwich panels. The objectives of this study were to: (1) design cellular cores for SPS bridge decks that are easy to manufacture; (2) investigate and compare the structural performances of CCSPs in accordance with the AASHTO LRFD Bridge Design Specifications for Strength I Limit State [22] using Finite Element Analysis (FEA); and (3) experimentally validate the computational model.

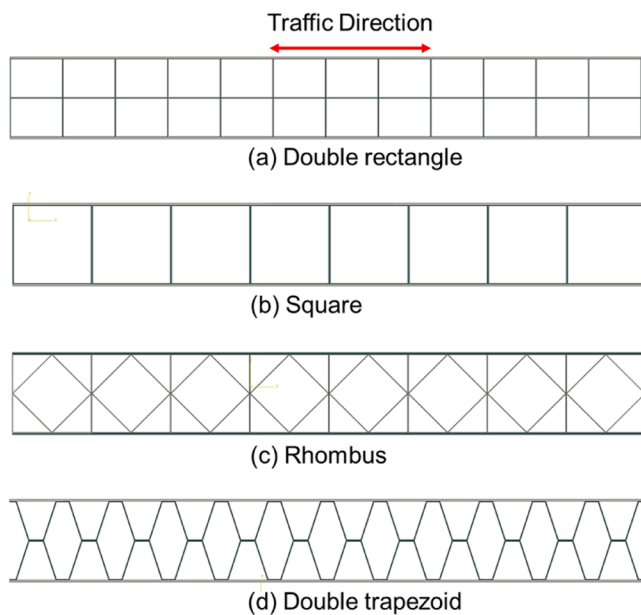


Fig. 1. The cross-section topology of CCSP models aligned parallel to the traffic direction. (a) Double rectangle, (b) Square, (c) Rhombus, and (d) Double trapezoid.

This paper is organized as follows. Section 2 describes the design of CCSP with different cell topologies. Section 3 discusses the FE modeling with loading and boundary conditions. Section 4 deals with the design of experiments for validation. Section 5 presents the experimental and computational results and compares the structural performances of different CCSP bridge decks. Section 6 discusses the limitations of the current study and its future directions.

2. Design of CCSP bridge deck

2.1. Sandwich panel cores

The most important aspect of a cellular solid is its relative density (ρ^*) defined as the ratio of the density of the cellular solid (ρ_c) to the density of the solid material that makes up the cell walls (ρ_s) [23]. In this study, four sandwich panel core architectures—double rectangle, square, rhombus, and double trapezoid (Fig. 1)—were designed in Solidworks (Dassault Systems, 2020), considering the availability of common commercial component shapes, ease of fabrication, and stress dissipation ability.

Double rectangle core unit cell consists of two 4×3 in. (0.102×0.076 m) rectangular cells stacking on each other. This cellular configuration enhances energy absorption, decreases the effective length to half the core thickness, reduces the buckling effect on the core, and thereby increasing the model's structural capacity.

Square core unit cell comprises a 6×6 in. (0.152×0.152 m) square tubing. It is the most straightforward core configuration where stress will be transferred vertically from the top to the bottom sheet by the vertical components acting like webs that theoretically generate higher stress concentrations and critical buckling effects than the competing counterparts. This model can be taken as a reference to compare the efficiency of the other investigated models.

Rhombus core unit cell consists of a 4×4 in. (0.102×0.102 m) rhombus tubing circumscribed in a 6×6 in. (0.152×0.152 m) square cell attached to the rhombus corners. This configuration is expected to distribute transverse load and stress vertically as well as diagonally within the core, producing wider stress dissipation and substantially higher bending stiffness.

Double trapezoid corrugated core consists of two corrugated sheets, each with a 3-in (0.076 m) crest, stacked above one another. This design is also intended to improve stress dissipation, enhance the buckling capacity, and achieve a high stiffness-to-weight ratio. While the top and bottom face sheet thicknesses were held constant throughout this study for each CCSP, the relative density (ρ^*) of the cellular core was varied by varying the cell wall thickness (t_c) according to the relationship shown below. The panels were evaluated for different relative densities between ~ 5 % and ~ 25 %.

$$\text{For double rectangle, } t_c = 1.6032\rho^* - 0.0674 \quad (1)$$

$$\text{For square, } t_c = 0.9856\rho^* - 0.0422 \quad (2)$$

$$\text{For rhombus, } t_c = 1.6773\rho^* - 0.0722 \quad (3)$$

$$\text{For double trapezoid, } t_c = 0.9492\rho^* - 0.0402 \quad (4)$$

2.2. Deck design specifications

The CCSP models in this study were designed to comply with the AASHTO LRFD Bridge Design Specifications (9th ed. 2020) for strength I bridge decks with infinite load-induced fatigue life, which designates HL-93 as the design truck load for bridge roadways [22].

Fig. 2 demonstrates the panel orientation with respect to the bridge girders and traffic flow, showing the loading configurations of an HL-93 truck for full and half axle loading. The sandwich panels will distribute the perpendicular out-of-plane live loads and dead loads to the parallel

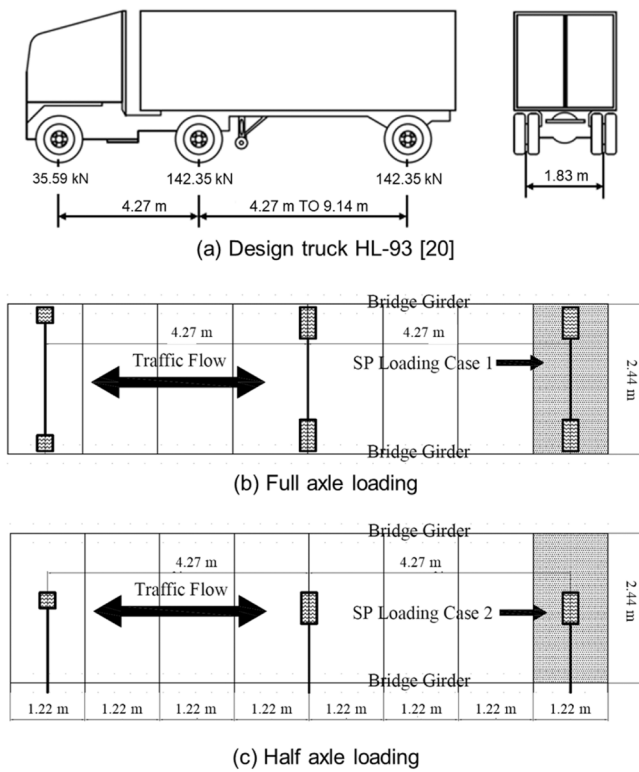


Fig. 2. Characteristics of the design truck HL-93 (a), orientation of sandwich panels on bridge superstructure and loading configurations for full axle loading (load case 1) (b) and half axle loading (load case 2) (c).

girders. Each panel was designed with a 4 ft (1.219 m) width, thus only one axle of the design truck will be positioned on each panel at any time. The overall sandwich panel dimensions for the model investigated in this study are 6" × 48" × 96" (0.152 m × 1.219 m × 2.438 m).

3. Finite element analysis

3.1. FE modeling and materials properties

Three dimensional (3D) CCSP bridge deck assembly with cellular core was modeled in Abaqus CAE v 6.14 (Dassault Systemes, 2014) with tie constraints between the surfaces. The surface-to-surface interaction results in a more uniform distribution of pressure within the tied interfaces. Each sandwich panel model was meshed with 3D hexagonal

(C3D8) element with full integration. The use of solid elements allowed for a more detailed representation of stress distributions and localized effects, particularly in regions of high stress gradients near connections and interfaces [24,25]. FE mesh convergence was achieved with 5 % variations in stress between two successive simulations. Mesh independence was achieved with a maximum element size of 0.5 in. (0.013 m). The aspect ratio was set to 10:1. All panels were designed with A36 steel, and the corresponding mechanical properties were considered in the FEA.

3.2. Boundary conditions

FE simulations were conducted based on two different scenarios—discontinuous (isolated, at the end) and continuous panels (panels connected to each other), and the boundary conditions (BCs) were applied accordingly. A pin connection between a CCSP deck panel and supporting girders represents a simply supported discontinuous panel (Fig. 3a). The other type of BC involved a pin connection between the panel and the girders contact areas, while fixing the ends of the panel to simulate a continuous bridge deck (Fig. 3b). A bolt connection between the deck sandwich panels and supporting girders was considered for the support-to-panel interaction for the support-to-panel interaction in the simulated models. This interaction between the support and the sandwich panel restrains the lateral displacement of the deck panels in all directions.

3.3. Loading conditions

The loading of a CCSP bridge deck comprises both dead load and live load. The dead load consists of the self-weight of the CCSP bridge deck with a uniformly distributed two-inch thick asphalt layer—145 lb/ft³ (2322.718 kg/m³) over the entire panel surface (Fig. 3c). The load combinations for the strength I limit state for the HL-93 design truck, as specified in the AASHTO LRFD bridge design specifications, were considered for the vehicular live load. The vehicular live load was determined from the HL-93 design truck combining the strength I limit state load as per the AASHTO LRFD bridge design specifications [22], as shown below:

$$Q = \sum n_i \gamma_i Q_i \tag{5}$$

where n_i is a load modifier, γ_i is load factor, and Q_i is equivalent to force effect originated from the loads. The load combination for Strength I Limit State is,

$$1.25 DC + 1.5 DW + 1.75 (LL + IM) \tag{6}$$

where DC is the components' dead load, DW is the future wearing

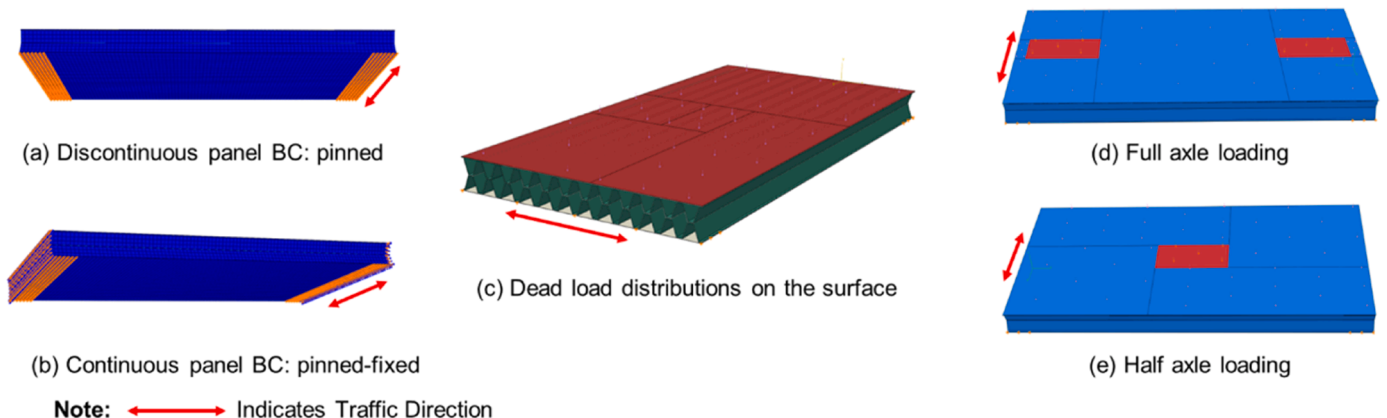


Fig. 3. (a) Discontinuous panel BC with pin supports, and (b) continuous panel BC with pin supports and fixed ends. Loading conditions represent (c) dead load distributions on the sandwich panel surface, (d) full axle loading (case 1), and (e) half axle loading (case 2), both displaying associated wheel contact area.

surface load, LL is the vehicular live load, and IM is the impact magnification factor. Two loading scenarios have been considered (Fig. 2) based on the wheel position of the design truck HL-93 on a CCSP panel—full axle (two wheels on the panel), and half axle (one wheel on the panel). Full wheel loads were applied directly over the sandwich panel upper surface in all the simulated models. 32 kips (142.345 kN) and 16 kips (71.173 kN) were considered for full axle (Fig. 3d) and half axle (Fig. 3e) loading conditions, respectively. Accordingly, the pressure exerted by the wheel contact area on a CCSP panel for a 32 kips (142.345 kN) axle load of the HL-93 design truck with the strength I magnification factors on two 20-inch \times 10-inch (0.508 m \times 0.254 m) wheel contact areas was calculated as 182.6 psi (1.259 MPa).

4. Experiments

To validate the FE simulation experimentally, a half scale sandwich panel with square cellular core of size 3-1/4" \times 24" \times 48" (0.083 m \times 0.610 m \times 1.219 m) was fabricated using A36 steel (Fig. 4a). The panel was fabricated carefully to avoid any major imperfection that may impact the experimental results. Similar to prior studies [26–31], a quasi-static three-point bending test was conducted using an MTS universal testing machine (UTM), in which the specimen was securely installed, ensuring proper alignment with an indenter of 6.5 in. (0.165 m) in diameter (Fig. 4b-c). The panel was supported by two perpendicular I beams located at the longitudinal ends of the specimen (Fig. 4b). A total of 40 kips (177.930 kN) was applied at the center of the panel at a rate of 200 lb/sec (90.718 kg/s) in cumulative sequences of 10 kips (44.482 kN) each until reaching the maximum of 40 kips (177.930 kN).

The vertical displacements at the center of the test panel and the in-plane strain at multiple locations were measured during testing (Fig. 5). The displacement was measured with two calibrated LP-200F Midori Precisions linear displacement sensors (DS) of 10 K Ohm resistance, and the strain was measured with six encapsulated Constantan-alloy of 120 OHM linear pattern strain gauges (SG). SGs 1–3 were installed on the bottom panel along the center line, with SG 2 in the mid center, as shown in Fig. 5b. Additionally, SG 6 was installed at the middle on right edge

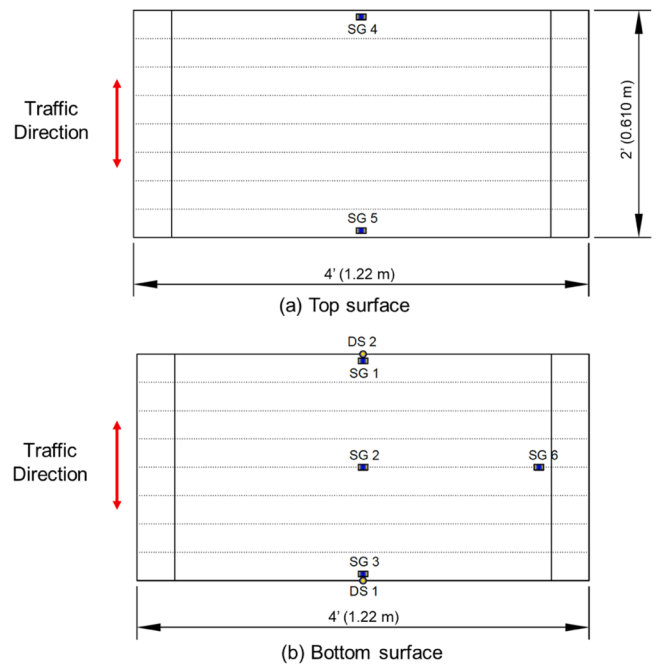
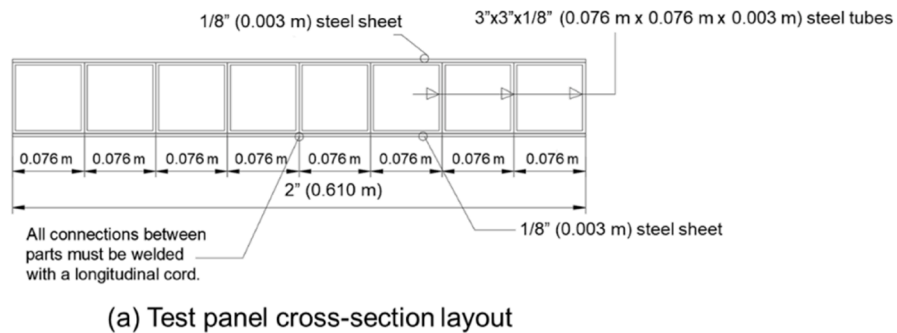


Fig. 5. Positions of the strain gauges and displacement sensors on the top (a) and bottom (b) surfaces of the test panel.

across the panel length. SGs 4 and 5 were installed on the top surface, which would be under compression (Fig. 5a) accordingly. DS 1 and DS 2 were installed on the bottom surface, aligned with SG 1 and SG 2, respectively (Fig. 5b). Strain Smart 7000 software was used to collect and monitor the real-time strains and displacements during the testing.

The FE simulation was validated by comparing with the experimental results obtained using the same boundary and loading conditions. The deflection and in-plane strain from the FE simulation were compared to those determined from the experimental study at identical locations on the experimental panel.



(a) Test panel cross-section layout



(b) Fabricated panel cross-section



(c) Test panel on the support

Fig. 4. (a) Test specimen cross-section layout (parallel to traffic direction), (b) Fabricated test panel cross-section viewed from the end, and (c) Longitudinal view of the specimen with its supports at the ends. The indenter is observed at the top.

5. Results and discussion

5.1. Comparison of experimental and FEA results

The FE model of CCSP with same core topology, material, loading, and boundary condition as the experimental model was simulated for the three-point bending test. The simulated maximum displacement (deflection) at the center of the panel and at the middle of edges across the width are 0.0787 in. (1.92 mm) and 0.069 in. (1.8 mm), respectively (Fig. 6a). The maximum tensile strain of 0.000847 and compressive strain of 0.000942 were found computationally at the center of the bottom and top face of the panel, respectively (Fig. 6b).

Table 1 compares the displacements obtained experimentally utilizing the displacement sensors (DS 1 and DS 2) at different load values up to 40 kips (177.93 kN) with those obtained from the finite element analysis. An average difference of 7 % was found, indicating a high level of agreement between the experiment and FE analysis results. Table 2 shows the strain variations between the FEA and experiment obtained via strain gauges. A high level of agreement was also evident for the strain responses, resulting in an average variation of only 3 % between the experiment and FE model.

5.2. Structural analysis for static loading

Each type of CCSP bridge deck was simulated for four different relative densities between 5 % and 25 % by varying the cell wall thickness (as per Eqs. 1–4) to assess their structural performance under static loading based on von Mises stress (yielding), shear stress, and maximum deflection. Each model was primarily simulated for both discontinuous (pinned) and continuous (pinned-fixed) boundary conditions and two different loading conditions—full (2) axle and half (1) axle.

5.2.1. Effect of boundary conditions

To assess the effect of discontinuous and continuous BCs (as shown Figs. 3a-3b), von Mises stress and deflections of the CCSPs were evaluated with both 2 (full) axle (Table 3) and 1 (half) axle (Table 4) loading conditions. For the CCSPs under 2 axle loading, the variations of von Mises stress and maximum deflection were 18 %-24 % and 27 %-29 %, respectively, between pinned and pinned-fixed BCs (Table 3). For the CCSPs under 1 (half) axle loading, the variations of von Mises stress and maximum deflection are 20 %-25 % and 33 %-37 %, respectively, between pinned and pinned-fixed BCs (Table 4). The pinned-fixed BC corresponds to the continuous panels exhibits lower von Mises stress as well as deflection in all the load cases in comparison with the responses of the pinned BC associated with discontinuous panels. This demonstrates that the pinned BC is critical and controls the strength capacity of the sandwich panels. Therefore, for conservative design, the pinned BC

was considered for further analysis. Furthermore, the results are shown at 10 % relative density, considering it as a low-density cellular core with thinner cell wall/strut to maximize the strength-to-weight properties.

5.2.2. Von Mises stress analysis of CCSP

Fig. 7 shows the von Mises stress distributions for each competing panel at 10 % relative density for full axle loading. Both the rhombus and double trapezoid panels, which have inclined strut/cell wall in their core configurations, exhibit a lower stress and a more efficient distribution of stress over a broader region on the panel's support. It is evident that these two cellular cores impart better structural performance than the double rectangle and square core sandwich panels. To be noted that the wheels are close to the panel support in the full axle loading case, and therefore, the high-stress regions are observed near the panel supports (girders).

Fig. 8 depicts the von Mises stress distribution for each competing panel for half axle loading, generating the maximum deflection at the center of CCSP, as observed in a three-point bending case. It is evident that both the rhombus and double trapezoid CCSP exhibit better structural efficiency under half axle loading by developing lower stress than the double rectangle and square core panels. However, the double trapezoidal model interestingly exhibited the highest bending stiffness at lower relative density, but lower bending stiffness at higher density than its counterparts.

Fig. 9 shows a nonlinear variation of von Mises stress in all CCSP models with relative density controlled by the cell wall thickness for full axle (Fig. 9a) and half axle (Fig. 9b) loading cases. All models exhibited a reduction in stress with increasing relative density; however, the rate of stress variation and stress magnitude depends on the core topology. It is apparent that the regression curves converge to their minimum stress at 20 % or higher relative density.

5.2.3. Shear stress analysis of CCSP

In the periodic cellular steel core sandwich panels, the low transverse rigidity of the core results in highly orthotropic structures for which shear deformations must be considered even at large length-to-depth ratios [1,32–35]. For this reason, we determined the maximum shear stress in the transverse cross-section caused by live load for both full axle and half axle loading cases. The nominal shear strength, V_n , as per the steel construction manual [36], was determined as follows,

$$V_n = 0.6F_y A_w C_{vl} \quad (7)$$

where F_y is the yield strength of steel, A_w is the web cross-section area of the element under shear stress, and C_{vl} is the web shear buckling coefficient. At 10 % relative density, $C_{vl} = 1.0$ for all models; thus, the allowable shear stress was calculated to 21.6 ksi (148.920 MPa).

Fig. 10 shows the shear stress distribution for the half axle loading

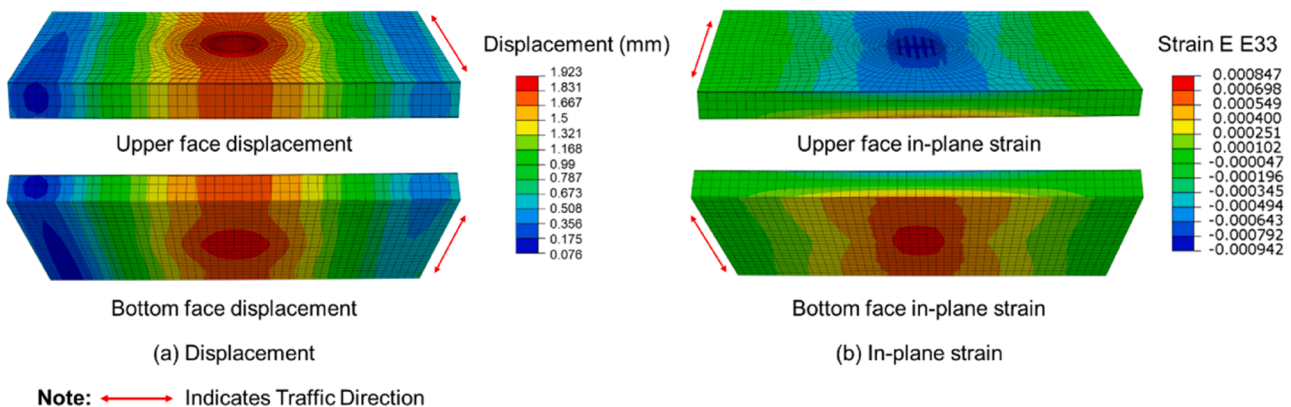


Fig. 6. Simulated displacement (a) and in-plane strain (b) found in the FE model of the test panel.

Table 1
Comparison of the displacement responses between the FE simulation and experiment.

Load (MPa)	SG 3	FEA	Variation (%)	SG4	FEA	Variation (%)	SG 5	FEA	Variation (%)	
17.79	0.000047	0.000048	1	-0.000057	-0.000056	1	-0.00006	-0.000056	6	
35.59	0.000092	0.000095	3	-0.000108	-0.000114	4	-0.000113	-0.000113	0	
57.83	0.000147	0.000150	2	-0.000169	-0.000178	5	-0.000176	-0.000178	1	
62.28	0.000164	0.000166	1	-0.00019	-0.000198	4	-0.000196	-0.000198	1	
80.07	0.000211	0.000214	1	-0.000241	-0.000254	6	-0.000249	-0.000254	2	
88.96	0.000233	0.000235	1	-0.000262	-0.000279	7	-0.000274	-0.000279	2	
97.86	0.000257	0.000262	2	-0.000285	-0.000311	9	-0.000300	-0.000311	4	
120.1	0.000318	0.000321	1	-0.000347	-0.000381	10	-0.000368	-0.000381	3	
133.45	0.000356	0.000357	0	-0.000384	-0.000424	10	-0.000409	-0.000424	4	
151.24	0.000409	0.000407	1	-0.00044	-0.000482	10	-0.000472	-0.000482	2	
160.14	0.000431	0.000428	1	-0.000474	-0.000508	7	-0.000499	-0.000508	2	
169.03	0.000457	0.000457	1	-0.00053	-0.000536	1	-0.000530	-0.000536	1	
177.93	0.000482	0.000476	1	-0.000681	-0.000564	17	-0.000561	-0.000564	1	
Average variation (SG 3)			1 %	Average variation (SG 4)			Average variation (SG 5)			2 %
Average strain variation in bottom surface										3 %

Table 2
Comparison of the in-plane strain between FE simulation and experiment.

Load (kN)	DS 1 (m)	FEA (m)	Variation (%)	DS 2 (m)	FEA (m)	Variation (%)	
57.83	0.000621	0.000553	11	0.000557911	0.00054168	3	
62.28	0.0007	0.000614	12	0.000652729	0.000600278	8	
80.07	0.000868	0.000774	11	0.000821436	0.000789457	4	
88.96	0.000942	0.000868	8	0.000888898	0.000851205	4	
97.86	0.001004	0.000943	6	0.000939114	0.000964921	3	
120.1	0.001266	0.001184	6	0.001114552	0.001160755	4	
133.45	0.001412	0.001316	7	0.001274013	0.001286434	1	
151.24	0.00166	0.0015	10	0.001407795	0.001470254	4	
160.14	0.001759	0.001579	10	0.001529283	0.001547647	1	
169.03	0.001927	0.001667	13	0.001675663	0.001629461	3	
177.93	0.002037	0.001754	14	0.001731289	0.0017145	1	
Average variation (DS 1)			10 %	Average variation (DS 2)			3 %
Average displacement variation in bottom surface							7 %

Table 3
Effect of BCs on different CCSP panels at 10 % relative density. Von Mises stress and maximum deflection for full axle loading.

Panel model	Core cell thickness (m)	Relative density (%)	Panel weight/Concrete weight	Pinned BC von Mises stress (MPa)	Fixed BC von Mises stress (MPa)	Stress variation (%)	Pinned BC max deflection (m)	Fixed BC max deflection (m)	Deflection variation (%)
DBL-REC	0.001372	10	30 %	141.344	102.609	27	0.001448	0.001143	21
RMB	0.001422	10	30 %	120.048	85.497	29	0.001143	0.000864	24
SQR	0.002413	10	30 %	164.16	117.921	28	0.001524	0.001245	18
DBL-TRAP	0.002286	10	30 %	104.012	75.218	28	0.001143	0.000914	20

Table 4
Effect of BCs on different CCSP panels at 10 % relative density. Von Mises stress and maximum deflection for half axle loading.

Panel model	Core cell thickness (m)	Relative density (%)	Panel weight/Concrete weight	Pinned BC von Mises stress (MPa)	Fixed BC von Mises stress (MPa)	Stress variation (%)	Pinned BC max deflection (m)	Fixed BC max deflection (m)	Deflection variation (%)
DBL-REC	0.001372	10	30 %	244.416	195.13	20	0.000559	0.000356	36
RMB	0.001422	10	30 %	191.673	145.936	24	0.000483	0.000305	37
SQR	0.002413	10	30 %	258.108	203.675	21	0.00061	0.000406	33
DBL-TRAP	0.002286	10	30 %	152.525	113.966	25	0.000483	0.000305	37

condition at the critical strut/cell wall of each CCSP along a longitudinal cut section. Since the square and double rectangle unit cells do not have any diagonal/inclined strut, the out-of-plane loads transfer vertically between the top and bottom surfaces, thereby generating higher shear stress in the critical struts. It is evident that double trapezoidal cellular core is more resistant to shear load compared to others in the full axle loading cases.

Fig. 11 shows the shear stress distribution for the half axle loading condition at the critical strut of each CCSP model along a longitudinal cut section. It is apparent that the rhombus (Fig. 11c) and trapezoid (Fig. 11d) core configurations dissipate shear energy more efficiently throughout the panel width along the cross-section, producing low localized shear stress at the center of the panel compared to the double rectangle and square CCSP under the same boundary and loading

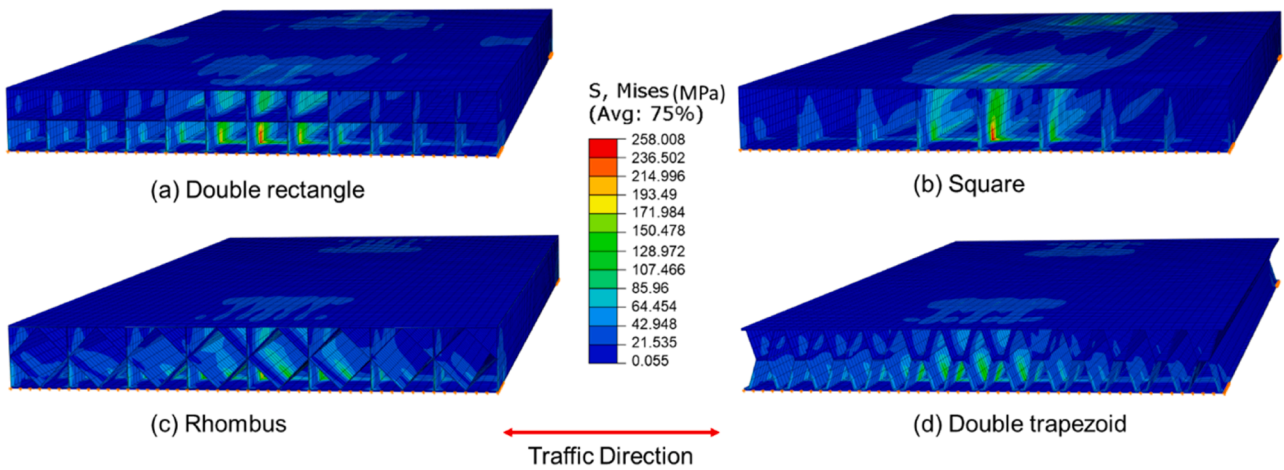


Fig. 7. Von Mises stress distribution in CCSPs with different core topology at 10 % relative density under full axle loading case. A common legend is used for comparison.

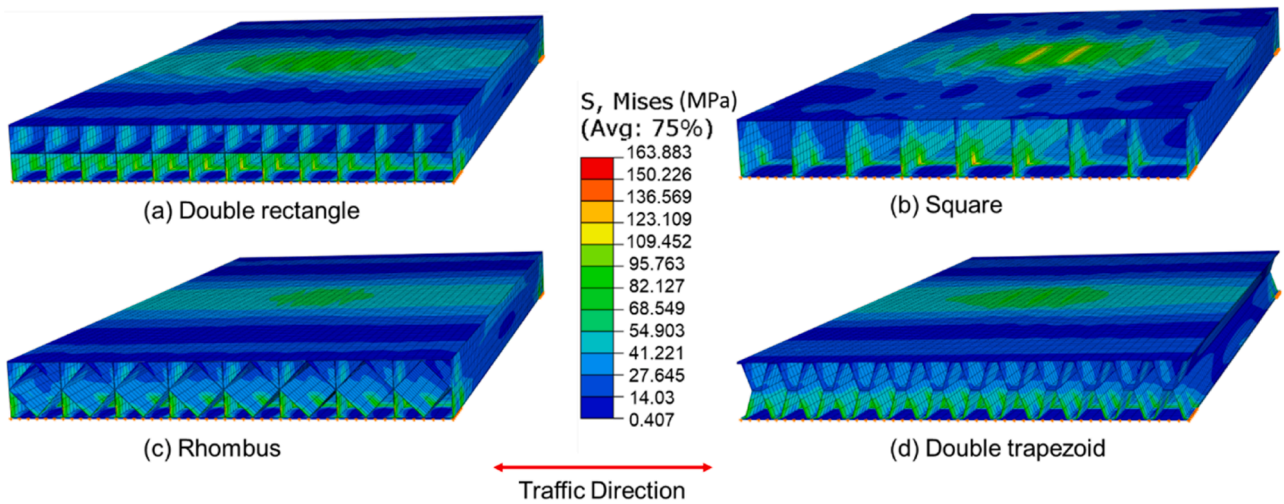


Fig. 8. Von Mises stress distribution in CCSPs with different core topology at 10 % relative density under half axle loading case. A common legend is used for comparison.

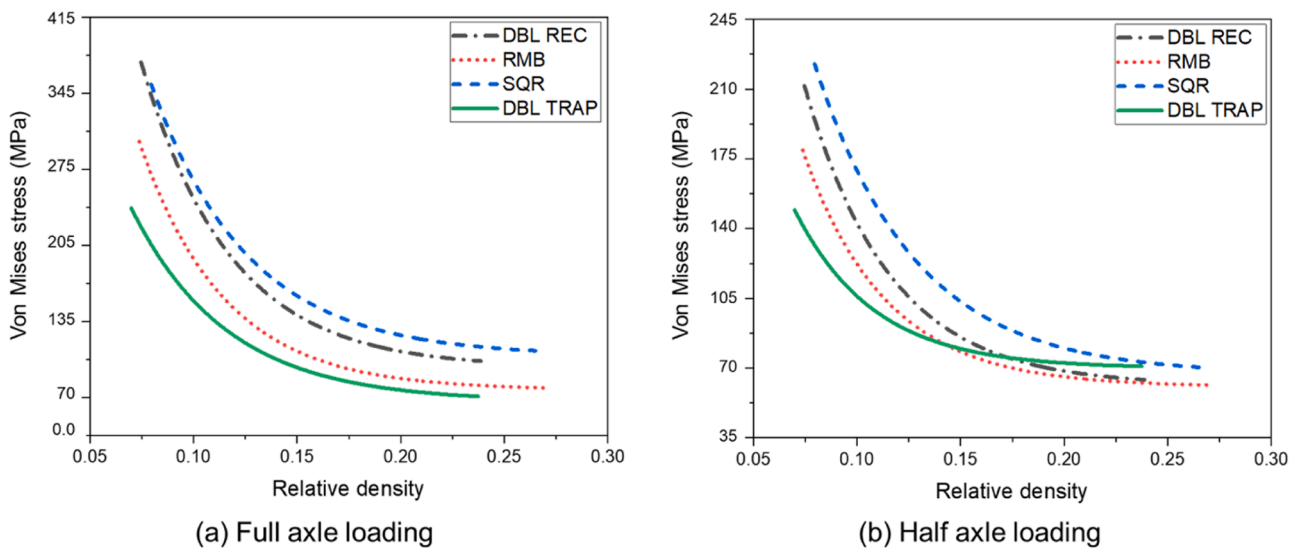


Fig. 9. Variation of von Mises stress with relative density of CCSPs with different cell topologies for full axle (a) and half axle (b) loading. DBL REC: Double rectangle, RMB: Rhombus, SQR: Square, and DBL TRAP: Double trapezoid.

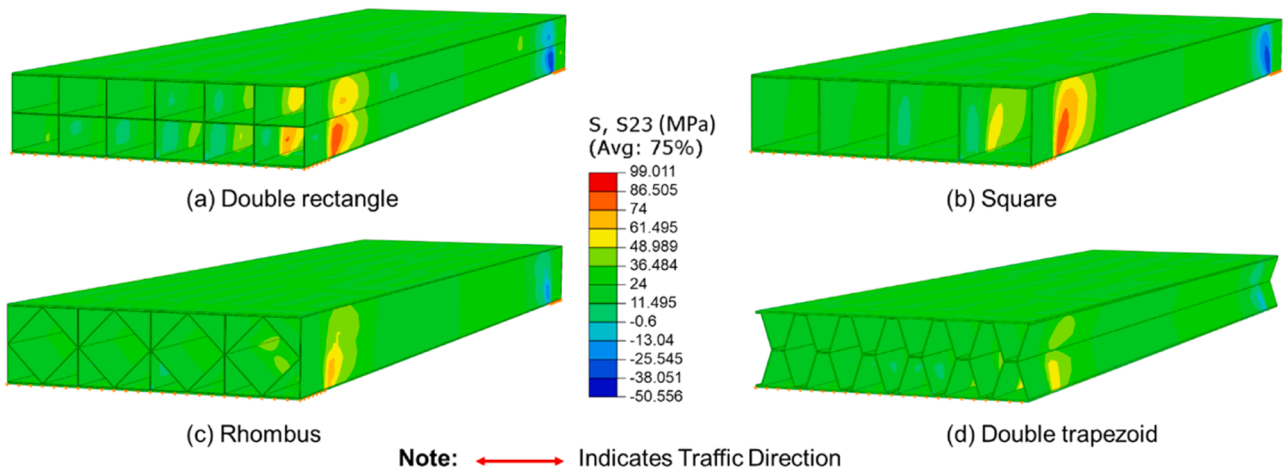


Fig. 10. Shear stress distribution (shown in longitudinal cut view for better representation) in panels for full axle loading. $\rho^* = 10\%$. A common legend is used for comparison.

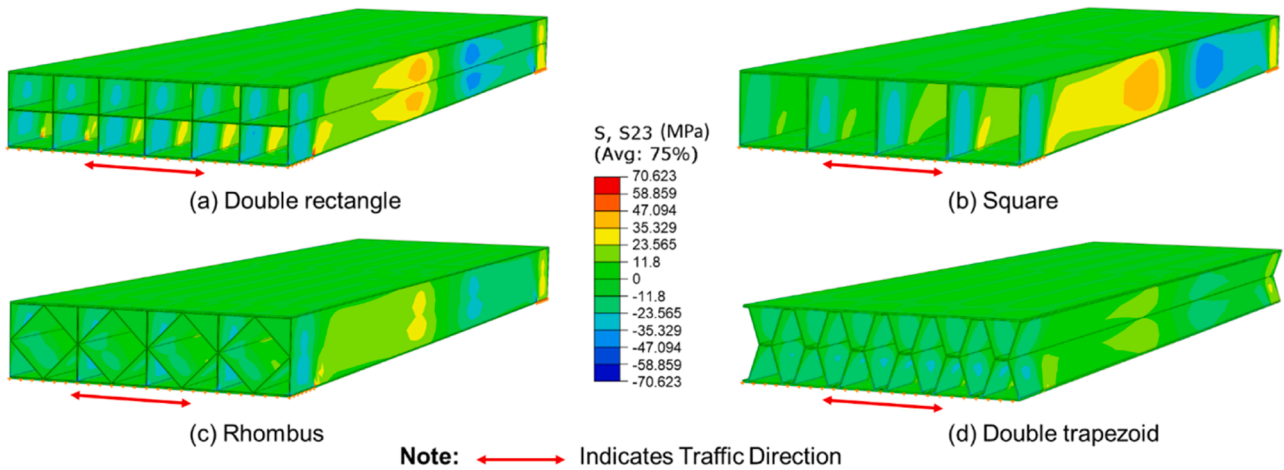


Fig. 11. Shear stress distribution (shown in longitudinal cut view for better representation) in panels for half axle loading. $\rho^* = 10\%$. A common legend is used for comparison.

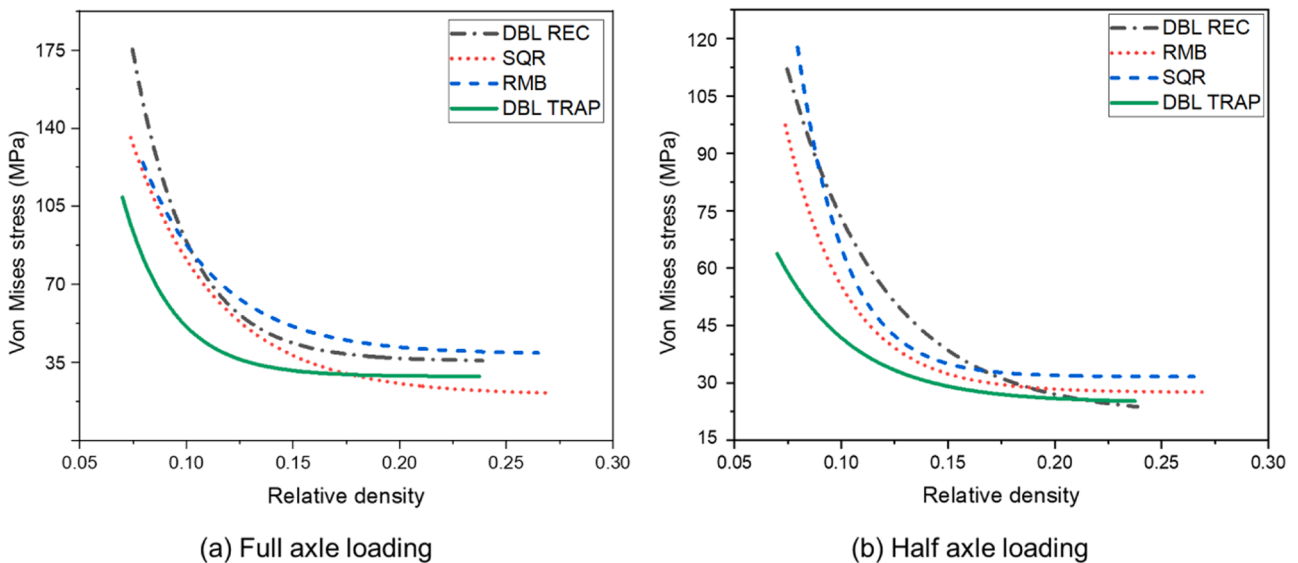


Fig. 12. Shear stress distribution in cellular panel with the relative density of CCSPs with different cell topologies for full axle (a) and half axle (b) loading. DBL REC: Double rectangle, RMB: Rhombus, SQR: Square, and DBL TRAP: Double trapezoid.

conditions. We observed that the full axle loading condition generated the highest shear stress in the sandwich panel cores, compared to the half axle loading condition.

A regression analysis was conducted to investigate the role of relative density of the cellular core on maximum shear stress for both full and half axle loading configurations (Fig. 12). Similar to the von Mises stress behavior, the shear stress decreases as the relative density or cell wall thickness increases. The double trapezoidal model exhibits lower shear stress at lower relative density than the other models, implying that the double trapezoid core model exhibits higher shear strength. However, for 17 % and higher relative density, the shear stress variation in the double trapezoidal panel is minimally sensitive to its relative density. Evidently, the square and double rectangle exhibit slightly better shear resistance at a higher relative density than the double trapezoidal model for both full and half axle loading. However, the shear stress is not as critical as the von Mises stress in causing yielding, as observed, and therefore, does not govern the CCSP design.

5.2.4. Deflection analysis of CCSP

The deflection of the sandwich panels due to live (full and half axle) load was assessed in accordance with AASHTO LRFD bridge design specifications [22]. In this work, we considered the maximum allowable deflection, $(L/1000)$ limit designated for *limited pedestrian traffic*, where L denotes the span length between the centers of the supports. The deflection responses of the panels subjected to the full axle loading are shown in Fig. 13. Since the wheel contact area is close to the supports in the full axle loading condition, the overall deflection in this load case is significantly low and does not impact the bending resistance of the sandwich panels. The predominant blue color in the deflection plots (Fig. 13) convincingly demonstrates that even the panels of 10 % relative density—considered very light weight—can easily satisfy the deflection limitations.

The one-wheel (half axle) loading condition was found to be critical for the bending stiffness of the sandwich panels. The 16 kips (71.173 kN) load of the half axle loading at the center of each panel resulted in a three-point bending loading condition that produced the highest deflection in the CCSPs. However, the maximum deflections (Fig. 14) for

10 % relative density panels are significantly lower than the allowable maximum deflections as per the AASHTO LRFD bridge design specifications.

Fig. 15 depicts the deflection behavior of the sandwich panels with varying cell wall thickness (relative density). It is evident that all models behave similarly—deflection reduces with the increase of cell wall thickness. Evidently, the unit cell without the diagonal element (square and double rectangle) deflected more than the double trapezoid and rhombus. It is apparent that the inclined struts help load dissipation that results in smaller deflections and higher bending stiffness.

5.3. Linear buckling analysis of CCSP

The static analyses showed a better structural performance for the CCSPs even with a core relative density of 10 %, which is considered to be a thin cell wall/strut that considerably lowers the panel’s dead weight. As the slenderness of the core element (struts) increases, the buckling phenomenon becomes a critical factor in the design of the sandwich panel. Local buckling due to transverse load creates an instability in the face sheet and/or the core cell walls. Instability in prismatic panels can occur when the core experience critical transverse compression or when panels are subjected to critical bending load from the transverse loading. Hence, a linear elastic buckling analysis was conducted for global and local buckling to determine the critical buckling load, represented by the minimum eigenvalue.

Figs. 16 and 17 show the buckling failure modes and eigenvalues generated with both full axle and half axle load cases, respectively. The full axle load exerted a transverse load that simultaneously generated both compression and shear stress at the core element as well as the at the outer face sheets. In contrast, the half axle load case, developing a 3-point bending condition, produced shear stress in the longitudinal direction of the core struts, which is critical for the global buckling of the sandwich panel. Fig. 16 shows the global buckling behavior of the CCSPs under the half axle loading with no critical buckling failure demonstrated by the high eigenvalues (Fig. 16). Local buckling is evident at the face sheet under the wheel contact area for the double rectangle, square, and double trapezoidal models (Figs. 17a, 17b, and 17d), but in the cell

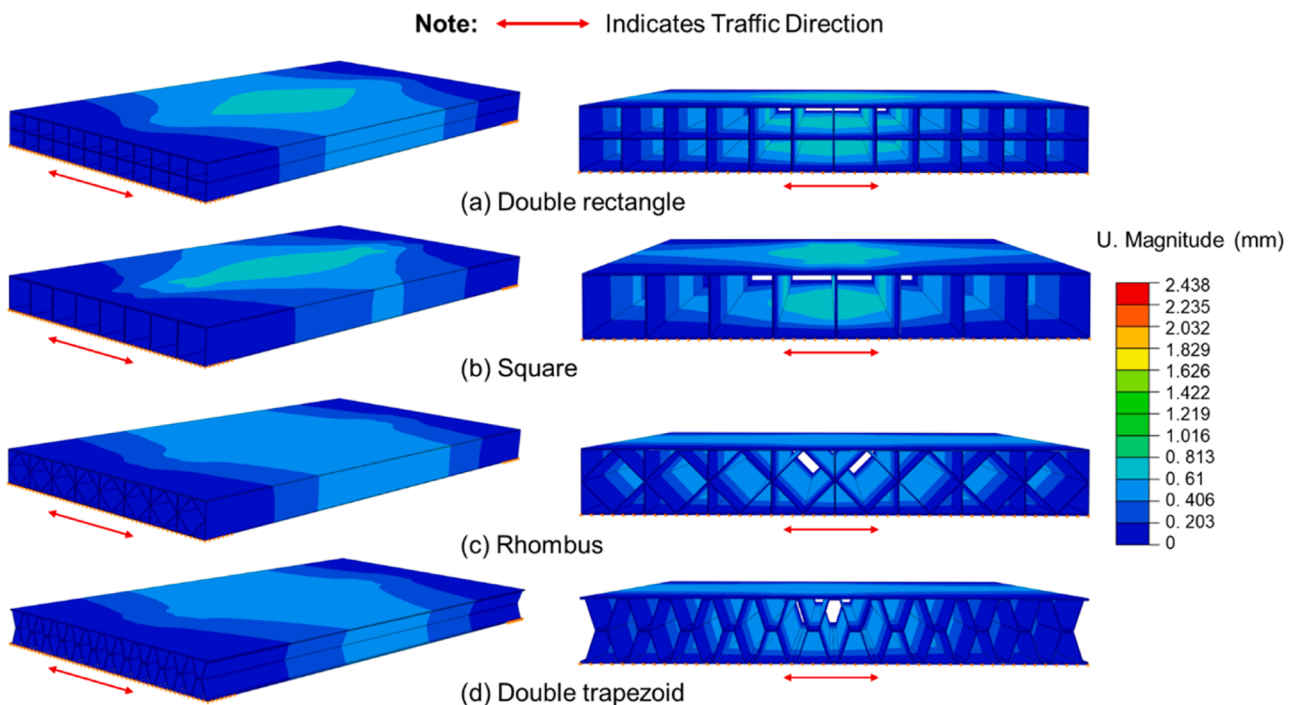


Fig. 13. Deflection contour plots for serviceability limit of $L/1000$ in CCSPs (isometric view at the left) and end view (right) under full axle loading. A common legend is used for comparison.

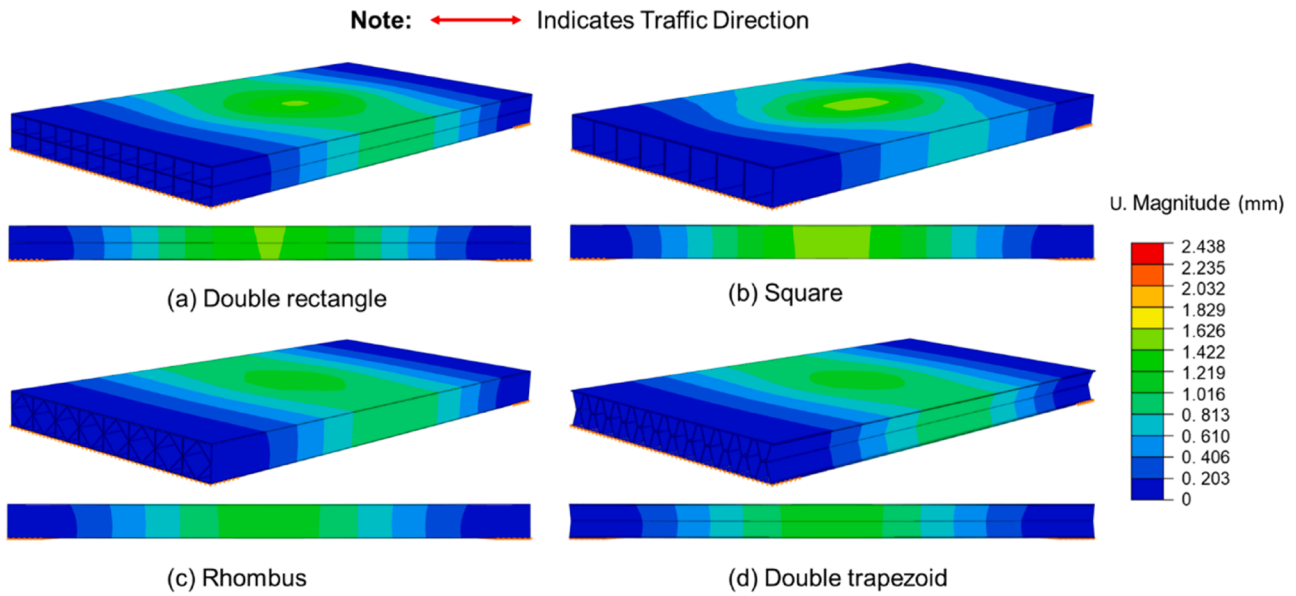


Fig. 14. Deflection contour plots for serviceability limit of $L/1000$ in CCSPs under half axle loading. A common legend is used for comparison.

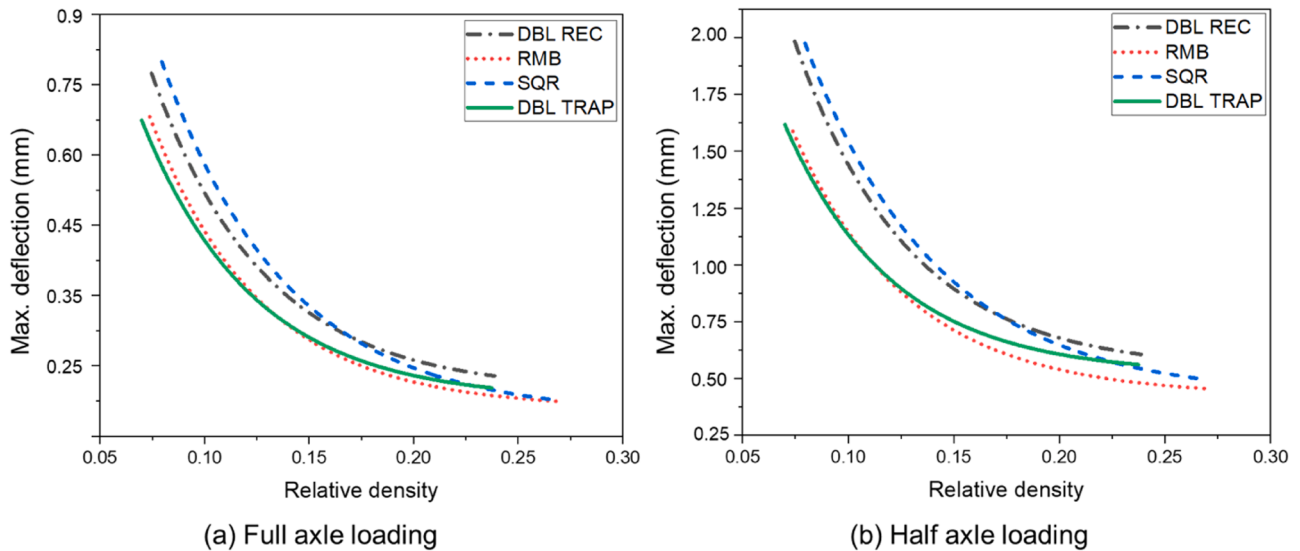


Fig. 15. Variation of the maximum deflection with the relative density of CCSPs for different cell topologies under full axle (a) and half axle (b) load cases. DBL REC: Double rectangle, RMB: Rhombus, SQR: Square, and DBL TRAP: Double trapezoid.

walls of rhombus core (Fig. 17c). However, the buckling failure has been found to be non-critical since all the eigenvalues are high enough for the sandwich panels, even at the 10 % relative density.

5.4. Fatigue analysis

One of the major problems for metal bridge decks is their fatigue life. Repetitive loading over an extended period of time may induce cracks well below the yield stress and promote crack propagation, potentially leading to premature failure of the structure that would otherwise be able to withstand equivalent loads under static conditions [37]. The fatigue life of the panels was determined by the stress at locations where high localized stress is generated. [38]. FE Safe module, coupled with Abaqus CAE, was employed for the fatigue life analysis, applying a sinusoidal cyclic loading with zero-based non-reversible alternating stress amplitude.

Goodman criteria [39,40] was employed to determine the life cycles

during the fatigue analysis conducted in FE Safe. The Goodman relation is expressed as follows:

$$\sigma_a = \sigma_w \left[1 - \left(\frac{\sigma_m}{\sigma_B} \right) \right] \tag{8a}$$

$$\sigma_a = A(N_f)^b \tag{8b}$$

where σ_a is stress amplitude, σ_w is the fatigue limit state, σ_m is the mean stress, σ_B represents unlimited tensile strength, A is the intercept of the accumulated stress at the endurance limit line, N_f is the number of cycles to fatigue failure, and b stands for the slope of the S-N fatigue life curve [41].

The fatigue life and durability of the sandwich panels subjected to the cyclic loading were determined to investigate that the CCSPs would be under serviceable condition throughout the assumed service life. Panels were subjected to the full axle loading conditions to determine the number of cycles before fatigue failure occurred. The fatigue

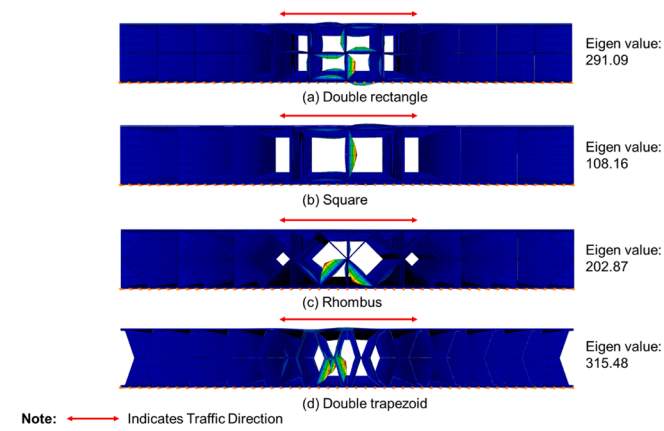


Fig. 16. Buckling failure modes in CCSPs under full axle loading, $\rho^* = 10\%$. (cross-section parallel to traffic direction).

responses illustrated in Fig. 18 show that the double trapezoid and square models will eventually fail by fatigue loading at a 10 % relative density. The rhombus and double trapezoid models at 10 % relative density do not exhibit any fatigue damage and consequently will have significantly better fatigue life. The half axle analysis showed no fatigue damage for any of the CCSPs.

6. Limitations and future research suggestions

6.1. Limitations of current research

While this study provides a comprehensive numerical analysis and an initial experimental validation of CCSPs as a proof-of-concept, several limitations need to be acknowledged. First, the study primarily focuses on idealized boundary conditions and loading scenarios, which may not

fully capture the complexities encountered in real-world applications. Additionally, the current research does not account for environmental factors such as temperature fluctuations, moisture, and long-term degradation, which can significantly impact material performance. Furthermore, the study lacks experimental validation of deck-girder connections, a critical element for ensuring composite action. Without detailed analysis or testing of interface shear mechanisms, such as headed shear studs or adhesive bonding, the practical implementation of the system remains speculative. Future studies should address these limitations by incorporating additional experimental investigations, exploring environmental effects, and refining numerical models to account for real-world uncertainties. Additionally, targeted research on connection methods will be essential to establish the feasibility and performance of these systems in bridge deck applications. Such efforts will enhance the practical viability and reliability of CCSPs in bridge deck applications.

6.2. Potential deck-girder connection

The connection between the deck and girder is critical to ensuring composite action and preventing slip under service loads. While the current study does not include specific research on deck-girder connections, possible solutions could involve the use of headed shear studs welded to the top flange of the girder and embedded into the deck panel. This approach is widely used in composite bridge design to provide shear resistance and facilitate force transfer. Another potential solution could involve the application of a high-strength epoxy adhesive layer, which can create a continuous bond across the interface, reducing stress concentrations associated with discrete connectors.

Future research should focus on the detailed analysis and experimental validation of these connection methods. This should include evaluating the shear transfer capacity, stress distribution, and long-term durability of the connections under cyclic and dynamic loads. Such

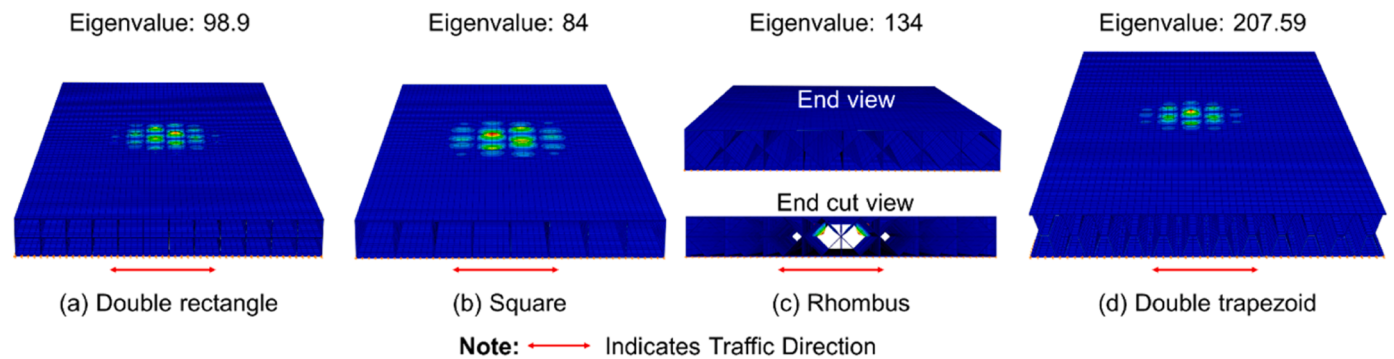


Fig. 17. Local buckling is observed at the face sheet of double rectangle (a), square (b), and double trapezoid (d) and in the cell walls of rhombus (end view (top) and end cut view (bottom) for a better representation) (c) of the CCSPs with 10 % relative density.

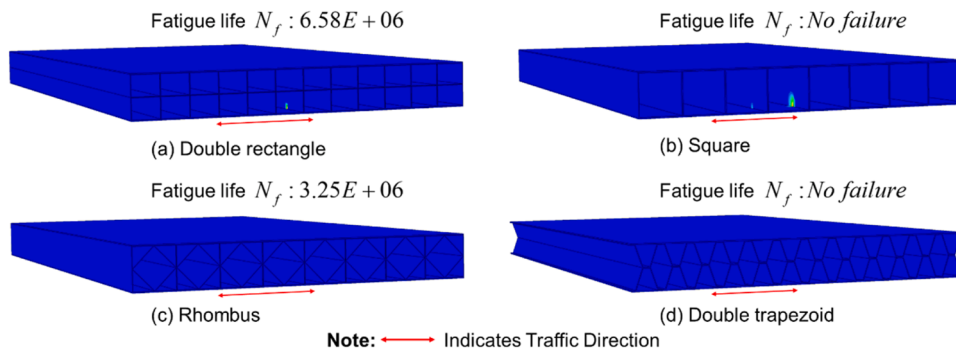


Fig. 18. Fatigue analysis of the CCSPs at 10 % relative density for full axle loading.

studies would provide critical insights into the practical implementation of this deck system in real-world bridge applications.

6.3. Future experimental validation of the deck system

Future research should also focus on expanding the experimental validation of the deck system by incorporating a variety of core shapes and connection methods. By designing and testing panels with different geometries, such as trapezoidal, honeycomb, and corrugated cores, under various loading and environmental conditions, additional insights into the practical performance of the system can be obtained. Moreover, long-term studies evaluating the durability, fatigue resistance, and interface shear behavior of these configurations would contribute significantly to understanding their feasibility for large-scale implementation in real-world bridge applications.

7. Conclusions

This study demonstrated that the influence of core topology on the structural performance of sandwich panels is significant and dependent on the behavior of core design. Although the core configuration impacts the shear failure as it transfers the shear load between the surfaces of the SPS [14], it is evident that the topology affects the overall structural capacity of a CCSP. Four easily manufacturable cell topologies were considered for designing lightweight cellular core sandwich panel for bridge decks to rehabilitate deteriorated bridge decks. This study showed that lightweight CCSPs can be an alternative to traditional bridge deck with comparable structural performance under static, buckling, and fatigue loading. A cell topology with inclined/diagonal cell walls/struts exhibited a higher stress dissipation capacity and higher structural strength than the cell with only vertical cell walls/struts. At 10 % relative density, the double trapezoid did not fail under any loading conditions investigated in this study. Furthermore, the construction utilizing CCSPs offers faster installation, reduces labor costs, and minimizes construction errors. Prefabrication and modular design will enhance their utility. Overall, sandwich panel decks can address structural weaknesses, increase bridge load capacity, enhance seismic resilience, comply with updated design codes, and improve existing bridge safety and service life. The rhombus and double trapezoid CCSPs proposed herein can be considered as a preliminary engineering solutions for new bridge decks and bridge deck replacements.

CRedit authorship contribution statement

Faisal Tanvir: Writing – review & editing, Writing – original draft, Supervision, Software, Resources, Project administration, Investigation, Funding acquisition, Conceptualization. **Hui Li:** Writing – review & editing, Validation, Methodology. **Khattak Mohammad J.:** Writing – review & editing, Supervision, Resources, Methodology. **Gopu Vijaya K:** Writing – review & editing, Project administration. **Alaywan Walid:** Writing – review & editing, Project administration. **Escoto Guillermo:** Investigation, Formal analysis, Data curation.

Declaration of Competing Interest

The authors declare the following financial interests/personal relationships which may be considered as potential competing interests: Tanvir Faisal reports financial support was provided by Louisiana Transportation Research Center. If there are other authors, they declare that they have no known competing financial interests or personal relationships that could have appeared to influence the work reported in this paper.

Acknowledgments

The authors gratefully acknowledge the financial support provided

by Louisiana Transportation Research Center TIRE Grant (Grant No. 23-3Tire/ DOTLT1000455). The authors acknowledge Md Saiful Islam for his help in postprocessing.

Data availability

Data will be made available on request.

References

- [1] Allen HG. Analysis and design of structural sandwich panels: the commonwealth and international library: structures and solid body mechanics division. Elsevier; 2013.
- [2] Lehman M. The American Society of Civil Engineers' report card on America's infrastructure. *Women in Infrastructure*: Springer; 2022. p. 5–21.
- [3] Teixeira de Freitas S. Steel plate Reinforced Bridge decks 2012.
- [4] Dackman D, Ek W. Steel sandwich decks in medium span bridges. Chalmers University of Technology; 2015.
- [5] Luchinsky DG, Hafiychuk V, Smelyanskiy V, Tyson RW, Walker JL, Miller JL. High-fidelity modeling for health monitoring in honeycomb sandwich structures. 2011 Aerospace Conference. IEEE; 2011. p. 1–7.
- [6] Vinson J.R. Sandwich structures. 2001.
- [7] Rejab M, Cantwell W. The mechanical behaviour of corrugated-core sandwich panels. *Compos Part B Eng* 2013;47:267–77.
- [8] Evans AG, Hutchinson J, Ashby M.J.P. Multifunctionality of cellular metal systems 1998;43:171–221.
- [9] Amazigo J, Budiansky B. Steady-state crack growth in supercritically transforming materials. *Int J Solids Struct* 1988;24:751–5.
- [10] Tatham R. Weight-Strength Analysis of Aircraft Structures. FR Shanley. McGraw Hill, New York 1952. 394 pp. Illustrated. 72s. 6d. net. *Aeronaut J* 1953;57:423.
- [11] Zaid N, Rejab M, Mohamed N. Sandwich structure based on corrugated-core: a review. *MATEC web Conf: EDP Sci* 2016:00029.
- [12] Vinson J.R. Sandwich structures: past, present, and future. *Sandwich Structures 7: Advancing with Sandwich Structures and Materials: Proceedings of the 7th International Conference on Sandwich Structures*, Aalborg University, Aalborg, Denmark, 29–31 August 2005: Springer; 2005. p. 3–12.
- [13] Ha NS, Lu G, Xiang X. Energy absorption of a bio-inspired honeycomb sandwich panel. *J Mater Sci* 2019;54:6286–300.
- [14] Charkaoui A, Hassan NM, Bahroun Z. Enhancing mechanical properties of cellular core sandwich panels: a review of topological parameters and design improvements. *Mater Res Express* 2023;10:102001.
- [15] Wadley HN. Cellular metals manufacturing. *Adv Eng Mater* 2002;4:726–33.
- [16] Alwan U, Järve D. New Concept for industrial bridge construction. Göteborg: Chalmers University of Technology; 2012.
- [17] Evans AG, Hutchinson JW, Ashby MF. Cellular metals. *Curr Opin Solid State Mater Sci* 1998;3:288–303.
- [18] Evans AG, Hutchinson JW, Fleck NA, Ashby M, Wadley H. The topological design of multifunctional cellular metals. *Prog Mater Sci* 2001;46:309–27.
- [19] Wadley HN. Multifunctional periodic cellular metals. *Philos Trans R Soc A Math Phys Eng Sci* 2006;364:31–68.
- [20] Zaid N, Rejab M, Mohamed N. Sandwich structure based on corrugated-core: a review. *MATEC Web Conf: EDP Sci* 2016.
- [21] Council NR. Aeronautical technologies for the twenty-first century. Academies Press. National; 1992.
- [22] AASHTO L. Bridge Design Specifications 9th edition (sn). Washington, DC: American Association of State Highway and Transportation officials; 2020.
- [23] Ashby MF, Gibson LJ. Cellular solids: structure and properties. Cambridge, UK: Press Syndicate of the University of Cambridge; 1997. p. 175–231.
- [24] Xue M, Cheng L, Hu N. The stress analysis of sandwich shells faced with composite sheets based on 3D FEM. *Compos Struct* 2003;60:33–41.
- [25] Potluri R, Raju MN, Babu KRP. Finite element analysis of cellular foam core sandwich structures. *Mater Today: Proc* 2017;4:2501–10.
- [26] Zenkert D. The handbook of sandwich construction. *Engineering Materials Advisory Services*; 1997.
- [27] Chang W-S, Ventsel E, Krauthammer T, John J. Bending behavior of corrugated-core sandwich plates. *Compos Struct* 2005;70:81–9.
- [28] Valdevit L, Wei Z, Mercer C, Zok FW, Evans AG. Structural performance of near-optimal sandwich panels with corrugated cores. *Int J Solids Struct* 2006;43:4888–905.
- [29] Xia F, Tan P, Ruan D. Failure mechanisms of corrugated sandwich panels under transverse three-point bending. *J Sandw Struct Mater* 2022;24:1808–27.
- [30] Xia F, Yu T, Durandet Y, Ruan D. Triangular corrugated sandwich panels under longitudinal bending. *Thin-Walled Struct* 2021;169:108359.
- [31] Romanoff J, Varsta P. Bending response of web-core sandwich beams. *Compos Struct* 2006;73:478–87.
- [32] Kujala P, Romanoff J, Tabri K, Ehlers S. All Steel Sandwich Panels-Design Challenges for Practical Applications in Ships. The Ninth Int Symposium on Practical Design of Ships and other Floating Structures, (PRADS 2004) Lubeck-Travemunde. Technical University of Hamburg-Harburg; 2004. p. 915–22.
- [33] Plantema F. Sandwich Construction: The Bending and Buckling of Sandwich Beams, Plates and Shells. New York: John Wiley; 1966.
- [34] Zenkert D. *Introd Sandw Struct* 1995.

- [35] Vinson J. [The behavior of sandwich structures of isotropic and composite materials](#). Routledge; 2018.
- [36] Construction AIOs. [American Steel Construction Manual](#). 16th Edition ed. Chicago2023.
- [37] Russo F.M., Mertz D.R., Frank K.H., Wilson K.E. [Design and evaluation of steel bridges for fatigue and fracture—reference manual](#). National Highway Institute (US); 2016.
- [38] [Fatigue design of bridges](#). 2023.
- [39] Sunca F, Ergün M, Altunışık AC, Günaydin M, Okur FY. [Modal identification and fatigue behavior of Eynel steel arch highway bridge with calibrated models](#). *J Civ Struct Health Monit* 2021;11:1337–54.
- [40] Wu J, Chen S, van de Lindt JW. [Fatigue assessment of slender long-span bridges: reliability approach](#). *J Bridge Eng* 2012;17:47–57.
- [41] Farhat H. [Operation, maintenance, and repair of land-based gas turbines](#). Elsevier; 2021.